3D probabilistic geology differentiation based on airborne geophysics, mixed L_p norm joint inversion and petrophysical measurements

Xiaolong Wei[1] and Jiajia Sun[1]

[1]Department of Earth and Atmospheric Sciences, University of Houston

Key Points:

- An efficient method is developed to quantify the uncertainties of 3D quasi-geology models.
- This method allows us to calculate the probability of geological units at any location in the model region.
- Our work, implemented using an open source framework, can be readily applied to many other regions and problems.

Corresponding author: Jiajia Sun, jsun29@central.uh.edu

Abstract

Geology differentiation converts physical property models derived from geophysical data to a 3D quasi-geology model. It represents a step change in quantitative interpretation of geophysical data. However, quantifying the uncertainties of the differentiated geological units in a 3D quasi-geology model has been largely unexplored. We have developed an empirical method to construct 3D probabilistic quasi-geology models in the deterministic inversion framework. We used mixed L_p norm joint inversion to recover a large sequence of physical property models based on multiple airborne geophysical data sets. Prior petrophysical measurements were used to determine the acceptance and rejection of these models. We then performed geology differentiation for all these accepted models and obtained a set of 3D quasi-geology models, based on which we constructed probabilistic 3D quasi-geology models. Our work has broad implications for 3D geological model building based on multiple geophysical and/or petrophysical measurements.

Plain Language Summary

Measuring and interpreting geophysical data has been the primary means of making inferences about subsurface structures and compositions. This practice typically produce physical parameter models (e.g., a density model of the subsurface Earth) as the outcome. Geology differentiation takes the physical property models derived from geophysics and output a 3D quasi-geology model that shows the 3D distribution of various geological units. It helps extract meaningful and useful geological information from geophysics and takes geophysics one step further into the realm of characterizing geology. However, assessing the uncertainties of a 3D quasi-geology model is lacking. This is critical as this answers the question as to how much confidence we can trust the 3D quasi-geology model. Our work fills such a gap. The fundamental idea of our work is to generate a large sequence of physical parameter models using an inversion method. Prior physical property measurements on rock samples are then used to accept only those models that fall within the range of measured values.

1 Introduction

Geophysical measurements contain important, sometimes the only information about the Earth's interior. Inversion is arguably amongst the most popular and effective interpretation methods that geophysicists have developed over the past few decades. The output of inversion is typically physical property models. Recently, Y. Li et al. (2019) discuss an approach, hereafter referred to as *geology differentiation*, that integrates geophysical inversion and geological classification into one unified framework. Geology differentiation takes multiple geophysical data sets as input and outputs a 3D quasi-geology model instead of physical property models. A quasi-geology model shows the 3D spatial distribution of various geological units. These geological units are defined by unique ranges of physical property values. A 3D quasi-geology model is a more useful and informative representation of the subsurface geology than physical property models. This approach has been applied to a multitude of geoscientific problems with promising results (e.g., Linde et al., 2006, 2008; Bedrosian et al., 2007; Doetsch et al., 2010; Infante et al., 2010; Martinez & Li, 2015; Devriese et al., 2017; Fournier et al., 2017; Kang et al., 2017; Melo et al., 2017; Kim et al., 2020; Giraud et al., 2020; Sun et al., 2020; Astic et al., 2021; K. Li et al., 2021).

However, uncertainty analysis of differentiated geological units in a 3D quasi-geology model is underexplored. The published works on uncertainty analysis have focused on quantifying the uncertainties of 1D and 2D physical property models in the Bayesian framework. Bayesian inferences for 3D inverse problems are rare and currently limited to several thousand (Zhang et al., 2018) model parameters. Latest work by (Manassero et al., 2020) reports 32,000 model parameters. Nevertheless, when it comes to 3D inverse prob-

lems that involve hundreds of thousands to tens of millions of model parameters, deterministic inversions still dominate and will dominate for years to come. A critical need exists to assess the uncertainties of 3D quasi-geology models constructed from geophysical measurements.

The objective of our work is to fill such a need by developing a deterministic approach to quantifying uncertainties of the differentiated geological units in a 3D quasi-geology model. To the best of our knowledge, our work is the first attempt to quantify uncertainties of 3D quasi-geology models derived from multiple geophysical data sets and prior petrophysical measurements. Our approach is based on established deterministic inversion theory (Fournier & Oldenburg, 2019) and an open-source framework *SimPEG* (e.g., Cockett et al., 2015; Heagy et al., 2017). We, therefore, believe that our work has broad and immediate impact on other researchers working in different regions or problems where multiple geophysical and petrophysical measurements exist. One such example is the use of gravity and magnetic data for volcano studies (e.g., Trevino et al., 2021; Miller et al., 2020). Another example is in mineral exploration where multiple airborne geophysical data sets are typically collected.

2 Methodology

Our method consists of two components: joint inversion and geology differentiation.

2.1 Mixed L_p norm joint inversion

Joint inversion aims to simultaneously invert multiple geophysical data sets in a unified mathematical framework. A commonly adopted objective function for joint inversion of two geophysical data sets is:

$$\Phi(\mathbf{m}_1, \mathbf{m}_2) = \Phi_{d1}(\mathbf{m}_1) + \Phi_{d2}(\mathbf{m}_2) + \beta_1 \Phi_{m1}(\mathbf{m}_1) + \beta_2 \Phi_{m2}(\mathbf{m}_2) + \lambda \Phi_c(\mathbf{m}_1, \mathbf{m}_2). \quad (1)$$

where $\mathbf{m}_1$ and $\mathbf{m}_2$ represent two different physical property models of interest. $\Phi_{d1}(\mathbf{m}_1)$ and $\Phi_{d2}(\mathbf{m}_2)$ are the two data misfit terms. $\Phi_{m1}(\mathbf{m}_1)$ and $\Phi_{m2}(\mathbf{m}_2)$ indicate the two regularization terms, and β_1 and β_2 are regularization parameters. $\Phi_c(\mathbf{m}_1, \mathbf{m}_2)$ is a coupling term allowing exchange of information between the two physical prorpety models. We adopted the cross-gradients coupling method (Gallardo & Meju, 2003) in our work. Our joint inversions were implemented using an open-source package *SimPEG* (e.g., Cockett et al., 2015; Heagy et al., 2017).

For the regularization terms $\Phi_{m1}(\mathbf{m}_1)$ and $\Phi_{m2}(\mathbf{m}_2)$, we used the mixed L_p norm regularization (Fournier & Oldenburg, 2019). It differs from the standard L_2 norm or L_1 norm regularization in that it allows different p norm values to be imposed on the different components of a regularization term, as shown below.

$$\Phi_{m1} = \alpha_{s1} \left\| \mathbf{W}_{s1} \mathbf{m}_1 \right\|_p^p + \sum_{i=x,y,z} \alpha_{i1} \left\| \mathbf{W}_{i1} \mathbf{m}_1 \right\|_q^q . \quad (2)$$

where p and q indicate the norm values imposed on the smallness and smoothness components, respectively. $\mathbf{W}_{s1}$ and $\mathbf{W}_{i1}$ ($i = x,y,z$) are the standard spatial weighting matrices for the smallness and the smoothness components. Scalars α_i ($i = s, x, y, z$) control the contribution of each component in the regularization term. When different p and q norm values are imposed, the resulting physical property models would show distinct features. For example, when $p = 1$ and $q = 2$, the resulting models would be both compact and smooth. The weights α_i ($i = s, x, y, z$) also affect the inverted models. More details on how different p, q and α_i ($i = s, x, y, z$) values affect the inverted models can be found in Wei and Sun (2021). Following Wei and Sun (2021), we fixed $q = 2$ and $\alpha_x = \alpha_y = \alpha_z = 1.0$ in our work.

2.2 Geology differentiation

When a pair of jointly inverted physical property models are obtained from the previous step, we perform geology differentiation. Specifically, we first summarize the jointly inverted physical property values (e.g., density contrast and susceptibility values) into a scatterplot. We then classify the inverted values into different units. Each unit should be characterized by a distinct range of physical property values. The classification is driven by several guiding principles. First, we look for well defined grouping patterns (e.g., clusters, linear trends) in a scatterplot. Each grouping feature is associated with a distinct range of physical property values, and therefore, can be considered as a unique unit. Secondly, the classified geological units, when visualized in 3D spatial domain, should match well-resolved inverted features obtained from joint (or, separate) inversions. Last but not the least, the classified units should be consistent with all available prior geological information, if any exists. Once the classification is completed, the final classified units can be visualized in 3D to produce a 3D quasi-geology model.

2.3 Probabilistic geology differentiation

The first step toward probabilistic geology differentiation is to generate a large sequence of 3D physical property models that all fit the observed geophysical data but exhibit a diverse range of features. To achieve that, we take advantage of the user-specified parameters in equation (2). Specifically, we randomly sample p and α_s multiple times. For each realization of (p, α_s) values, we perform one joint inversion by minimizing the objective function in equation 1.

In the second step, we use prior petrophysical information to determine the acceptance and rejection of the inverted models. The reason is that some of the models fall outside of the ranges of the physical property values measured on the drill core samples. Only these models that are consistent with both geophysical and petrophysical measurements proceed to the next step. In the third step, we perform geology differentiation following the guiding principles described in the previous section and construct a 3D quasi-geology model for each of the accepted model pairs, based on which we calculate the probability of the spatial distribution for each unit as well as the probability of geological units at each location. Fig. 1 summarizes our workflow of constructing probabilistic quasi-geology models.

3 Geophysical and petrophysical measurements

Our study area, located in the border of northeast Iowa and southeast Minnesota, is characterized by a thick sedimentary layer underlain by Precambrian rocks according to published work (e.g., Drenth et al., 2015; Sun et al., 2020) and drillhole sample measurements (Fig. 2a). The magenta and blue curves in Fig. 2a represent the measured density and susceptibility values based on rock samples from drillhole BO-1. The light yellow area represents sedimentary rocks and weathered basement, where we can observe relatively low density and susceptibility values. The gray area in Fig. 2a is associated with Precambrian basement rocks with higher density and susceptibility values. The lower and upper bounds of density values for Precambrian basement rocks are 0.43 and 1.11 g/cm^3, respectively, and the bounds of susceptibility values are 0.115 and 0.495 SI. These two ranges, [0.43 g/cm^3, 1.11 g/cm^3] and [0.115 SI, 0.495 SI] were later used to help us determine which models to accept and reject. Fig. 2b and c display the measured airborne gravity gradient and magnetic TMI data, respectively.

4 Deterministic geology differentiation

The data sets shown in Fig. 2b and c were used to perform 162 joint inversions. We now use one such inversion with p=0.25 and α_s=0.03 to explain how geology differ-

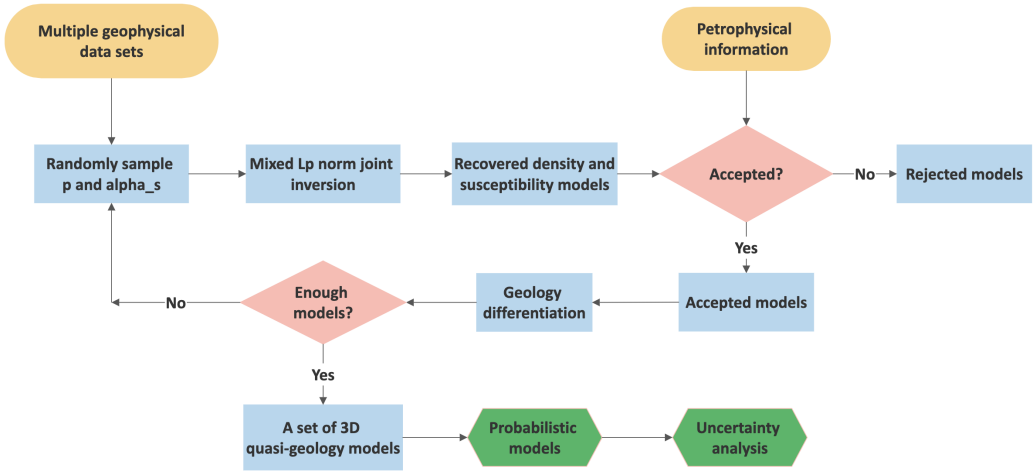

Figure 1. Our workflow of constructing probabilistic quasi-geology models based on multiple airborne geophysical data sets. Mixed L_p norm joint inversion is used to recover density and susceptibility models. Petrophysical measurements on drill core samples are used to determine the acceptance and rejections of the jointly inverted models.

entiation was performed. The jointly recovered density (Fig. 3a) and susceptibility (Fig. 3b) values were summarized into a scatter plot, and classified into 9 geological units marked as 9 different colors in Fig. 3c. We visualized the classification results in 3D spatial domain and obtained a 3D quasi-geology model. A depth slice at 2,000 m and a vertical cross-section at 4820000 m extracted from the 3D quasi-geology model are shown in Fig. 3d. For ease of explanation, we overlaid the boundaries of the differentiated units (as solid and dashed lines) on the jointly recovered density (Fig. 3e-1 to e-4) and susceptibility (Fig. 3f-1 to f-4) models. The boundary of Unit 1 is not shown because Unit 1 is interpreted as the background. A 3D visualization of the remaining 8 units can be found in the Supplemental Materials (Figures S1-S8).

4.1 Unit 2

Unit 2 is defined by intermediate negative susceptibility values and near-zero density contrast values (Fig. 3c). When visualized in 3D spatial domain, Unit 2 appears as one NE-SW trending feature and several isolated small anomalous bodies, as delineated by the solid black lines in Fig. 3e-1 and f-1. The NE-SW trending feature is likely to be associated with granitic plutons which usually produce large magnetic but weak gravity anomalies. According to Drenth et al. (2015), these granitic plutons are part of a large swath of anorogenic magmatism extending from the southwestern United States northeast to the Nain Plutonic Suite in Labrador (e.g., Anderson, 1983; Ashwal, 2010, 2013).

The isolated small bodies are harder to interpret. For example, the size of the tiny body indicated by the black arrow in Fig. 3e-1 and f-1 is simply too small, when compared with the spatial resolution of airborne geophysical data, to be reliably recovered. This feature is, therefore, very likely an artefact. Likewise, the compact body indicated by the red arrow is characterized by near-zero density contrast and susceptibility values, and are more likely to be part of the background (i.e. Unit 1). Indeed, if we moved the lower bound of Unit 1 (i.e., the bound between Units 1 and 2 in Fig. 3c) downward to include some of the small susceptibility values, this body would have been classified into Unit 1. This highlights the importance of developing an assessment of the probability of the classified units, instead of relying on a single classification outcome.

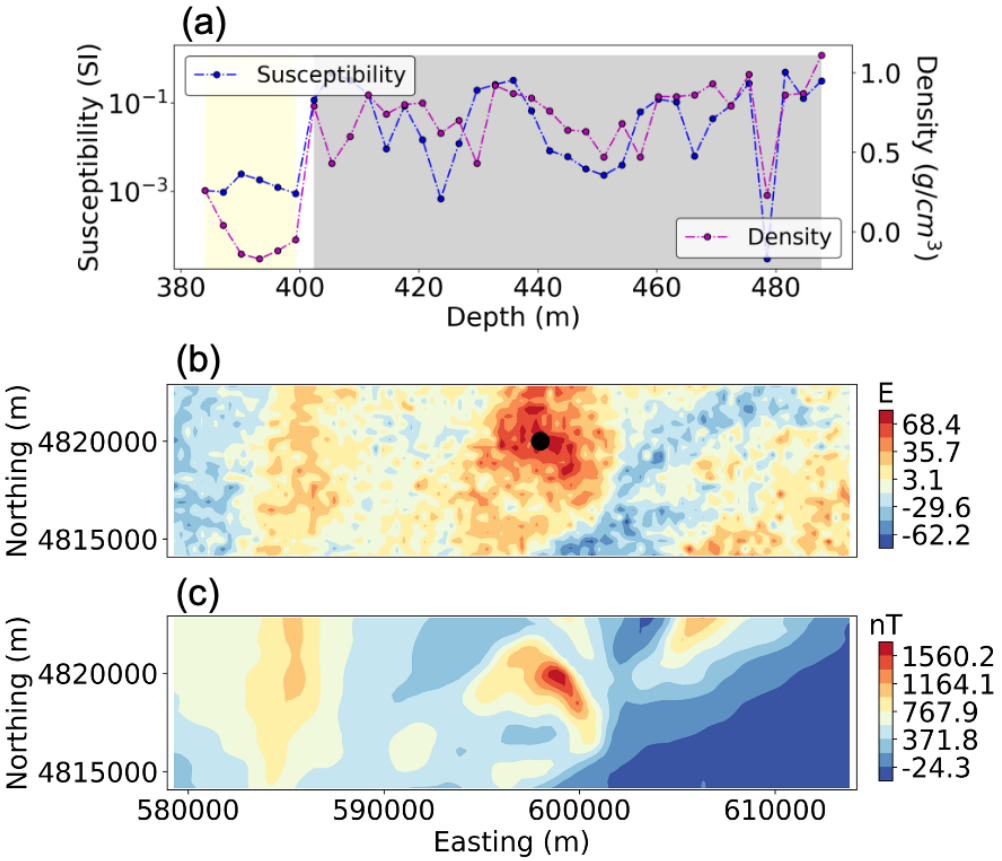

Figure 2. (a) Measured density contrast (magenta dots) and susceptibility (blue dots) values based on rock samples from drillhole BO-1. Density contrast values were obtained by subtracting a background density of 2.4 g/cm^3. The local minimum density and susceptibility values at the depth of about 480 m, are determined to be outliers, and are excluded from the rest of our work.(b) The observed airborne gravity gradient data, where the black dot represents the drillhole location. (c) The observed airborne magnetic TMI data.

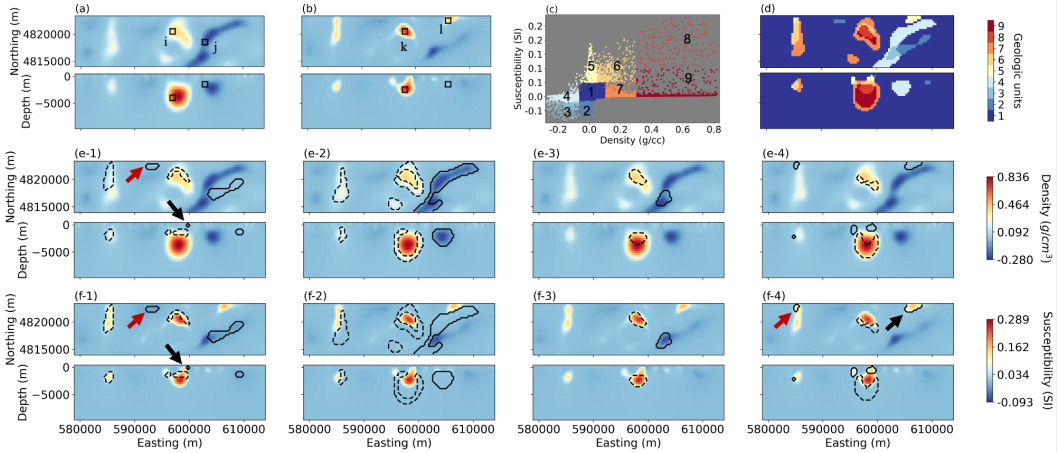

Figure 3. Recovered density (a) and susceptibility (b) models from a mixed L_p norm joint inversion with p=0.25, α_s=0.03. The black boxes, labeled as i, j, k and l, represent the spatial locations discussed in Section 5.3. (c) The recovered values are classified into 9 distinct units. (d) The corresponding 3D quasi-geology model visualized as a depth slice at -2000 m (top) and cross section at 4820000 m (bottom). From e-1 to e-4, the solid lines indicate boundaries of Unit 2, 3, 4 and 5; dashed lines represent boundaries of Unit 6, 7, 8 and 9. The boundaries shown in f-1 to f-4 are consistent with e-1 to e-4.

4.2 Unit 4

Unit 4 consists of intermediate negative density and around-zero susceptibility values. When visualized in spatial domain, Unit 4 corresponds to a NE-SW trending feature indicated by the whitish color in Fig. 3d. In Fig. 3e-2, Unit 4, whose outline is delineated as solid black lines, spatially coincides with the well-defined negative density anomalous feature trending NE-SW. Following Drenth et al. (2015), we interpret Unit 4 as a silicic pluton that typically produces strong negative gravity response and very weak magnetic responses.

4.3 Unit 3

Unit 3 is characterized as intermediate negative density contrast and susceptibility values. This unit corresponds to an isolated body whose boundary is delineated as the solid black line in jointly recovered density (Fig. 3e-3) and susceptibility (Fig. 3f-3) models. Unit 3 is located at the intersection of the two NE-SW trending features in Units 2 and 4, as shown in Fig. 3d. Interestingly, the geophysical characteristics of Unit 3 also seems to be a mix of those from Units 2 (negative susceptibility) and 4 (negative density contrast). One possible explanation is, when Unit 2 intruded Unit 4, the magnetic minerals in Unit 2 and the silica in Unit 4 interacted to form Unit 3. Considering the relative small volume of Unit 3, it is legitimate to ask if it is a real feature or an artefact. This again served as a motivation for our work.

4.4 Unit 5

Unit 5 is dominated by intermediate to high positive susceptibility and near-zero density values. Therefore, we interpret Unit 5 to be associated with granitic intrusions, similar to Unit 2, but with normal magnetic polarities. In the recovered density (Fig. 3e-4) and susceptibility (Fig. 3f-4) models, Unit 5, marked as solid lines, consists of several isolated compact bodies. Some of them might be artifacts, because they appear at the boundaries of some well-defined anomalies. For example, the small body indicated by red arrow (Fig. 3f-4) is at the boundary of a well-defined linear feature trending N-S. This small body might be simply due to the smoothness regularization in equation 2 where q is set to 2, or due to the subjectivity involved in our manual geology differentiation. Without some assessment of the uncertainties, it is difficult to tell if this feature is real or not.

Description of Units 6-9 can be found in Text S1 in the Supplemental Materials. The above analysis clearly reveals a need to quantify the uncertainties of the differentiated units.

5 Probabilistic geology differentiation

5.1 A sequence of 3D quasi-geology models

We randomly generated 162 pairs of (p, α_s) values with $p \in [0, 2]$ and $\alpha_s \in [0.01, 1]$. Figure S9 in the Supplemental Materials summarizes all the 162 combinations. We then implemented 162 mixed L_p norm joint inversion and obtained 162 pairs of jointly recovered density and susceptibility models. The prior density and susceptibility measurements shown in Fig. 2(a) were used to determine the acceptance and rejection of these recovered models. We rejected those models whose inverted values at the drillhole location are outside of the measured physical property ranges. Text S2 and Figures S10, S11 in the Supplemental Materials details rejection procedure. Following this criteria, only 37 pairs of jointly inverted density and susceptibility models were accepted for subsequent geology differentiation and uncertainty analysis. Figure S12 shows several examples of accepted and rejected models. We note that the jointly inverted models based on L_p norms, where p is close to 2.0, are all rejected because their recovered physical property values are overly underestimated and lower than the acceptable ranges (see the third row in Figure S12). The red dots in Figure S9 represent those (p, α_s) values for the accepted physical property models. For each accepted pair of density and susceptibility models, we performed geology differentiation and obtained 37 accepted quasi-geology models. Below, we quantify probabilities of spatial distributions for each geologic unit and calculate probabilities of geological units at any location in our study area.

5.2 Probabilities of the spatial distribution of geological units

Each unit in a quasi-geology model can be converted to a binary model, where 1 and 0, respectively, represent the anomalies and background. We thus obtained a total of 37 binary models for each geologic unit in which the frequency of the 1s at each model cell indicates the probability of this geologic unit. Figure S13 and Text S3 in the Supplemental Materials explain how we obtained the probabilities of the spatial distribution for Unit 2. The same procedure was applied to all the other units.

Fig. 4a-h display the probabilities of each geologic unit excluding the background Unit 1. The warm and cold color of Fig. 4 indicate the high and low probabilities, respectively. We observe that the NE-SW trending feature in Unit 2 (Fig. 4a) has high probabilities, indicating that most of our recovered physical property models and quasi-geology models agree with each other on the spatial distribution of this feature. But, the two isolated bodies highlighted by the red and black arrows in Fig. 3e-1 and f-1 are as-

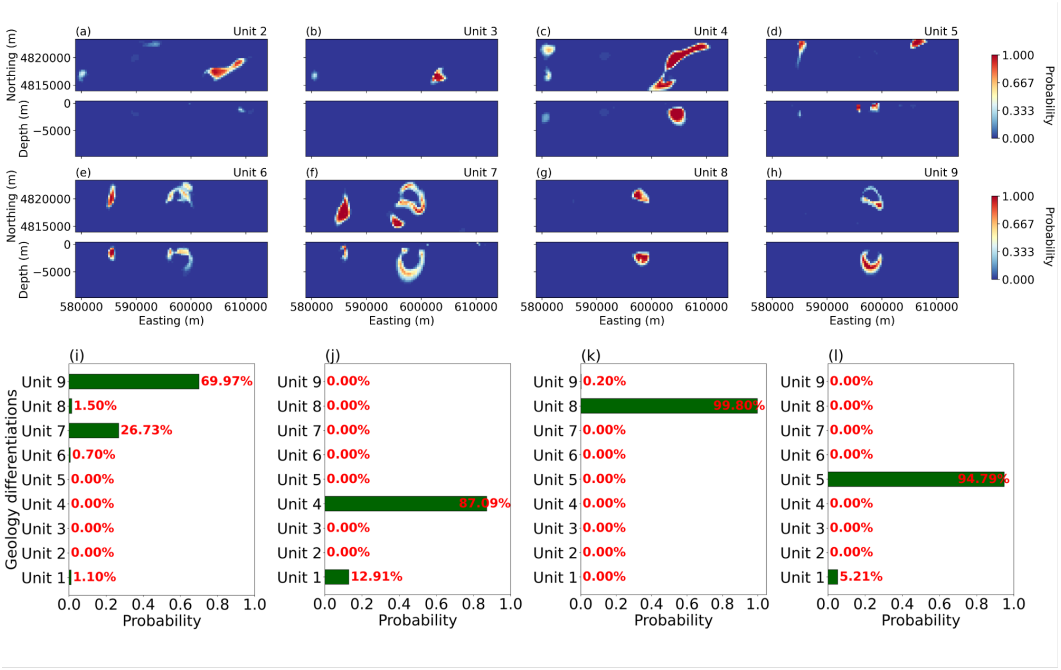

Figure 4. The probabilities of spatial distribution for geological units. Unit 2 to 9, excluding Unit 1 which is background, are mapped on (a) to (h) accordingly, where warm and cold colors, respectively, represent high and low probabilities. (i) - (l) display probabilities of geologic units at different spatial locations indicated by black boxes in Fig. 3a and b.

sociated with very low probabilities, indicating that there exists a high level of variability, and therefore, uncertainty, among the accepted inverted models and quasi-geology models. Therefore, these two isolated bodies are not reliable features and should be interpreted with caution. In the probability model for Unit 4 (Fig. 4c), the NE-SW trending feature is also characterized by high probabilities compared with the two isolated anomalous bodies located in the west. We thus are more confident in spatial extents of the trending feature, and less confident in the existence of two western anomalous bodies. Unit 5 (Fig. 4d) consists of multiple small anomalous bodies. In Fig. 3e-4 and f-4, these small anomalous bodies, outlined by solid lines, are located at the boundaries of some prominent features. However, the probability model (Fig. 4d) indicates that these small anomalous bodies are more likely to be true geological features because of their high probabilities. Both Unit 6 (Fig. 4e) and 7 (Fig. 4f) display a wider range of probabilities, with the western intrusion having higher probabilities and central anomalous bodies associated with intermediate to low probabilities. The probability models for Unit 8 (Fig. 4g) and 9 (Fig. 4h) show that the spatial extents of these two units are well defined. The probability maps in Fig. 4a-h provide empirical estimates of the uncertainties of the spatial distribution for each unit. They constitute a critical piece of information that allows uncertainty to be taken into account when it comes to interpretation and decision making (e.g., where to drill).

5.3 Probabilities of geological units at spatial locations

We also computed the probabilities of geological units at each spatial location (e.g., at each model cell). This probability quantifies the likelihood of a model cell belonging to each of the 9 differentiated geological units. We achieved this by computing the unit

number assigned to a model cell by all the 37 quasi-geology models. Fig. S14 and Text S4 in the Supplemental Materials explains how this was carried out in our work.

As an illustration, we selected two locations at the boundaries of the central anomalous body and the NE-SW trending feature. These two locations are marked as black boxes in Fig. 3a and labeled as i and j, respectively. The probabilities of geological units at these two locations are shown in Fig. 4i and j, respectively. We observe that the probability of location i belonging to Unit 9 is 69.97%, and the probability for Unit 7 is 26.73%. At the location j, the geologic unit is likely to be Unit 4 with a probability of 87.09%. But there is also a 12.91% probability of belonging to Unit 1. We also chose another two locations at the core areas of two geological features, as shown by the black square boxes labeled as k and l in Fig. 3b. Our probabilistic geology differentiation results in Fig. 4k and l indicate that the location k is almost certainly associated with Unit 8 (with 99.80% probability), and the location l has a probability of 94.79% belonging to Unit 5. Similar quantitative and probabilistic interpretations can be made at any locations. Movie S1 displays our probabilistic geology differentiation results at multiple locations.

6 Discussions

Bayesian inferences are commonly used in geophysics to quantify uncertainties. Despite its successful applications in many problems, it suffers from the curse of dimensionality and is computationally prohibitively expensive especially when it comes to 3D inverse problems. Literature search shows that Monte Carlo sampling methods can typically handle several hundred to thousand model parameters, and the computational time currently ranges from several weeks to months (Piana Agostinetti & Bodin, 2018; Zhang et al., 2018; Manassero et al., 2020) even with parallelization. To the best of our knowledge, Monte Carlo sampling methods have not been applied to 3D joint inverse problems yet. This is not surprising because joint inversion is typically much more time consuming than separate inversion.

Our work is based on a fundamentally different approach. We use a deterministic inversion method recently developed by Fournier and Oldenburg (2019) to generate a large sequence of equivalent models by adjusting two user-specified parameters, p and α_s. Despite being empirical in nature, this method allows us to generate many equivalent models in a reasonable amount of time for large scale 3D problems. In our work, there are a total of 287,100 unknown model parameters and 8,968 observations. Inverse problems of this size are currently out of reach for Monte Carlo sampling methods. We completed 162 joint inversions within three weeks on a computer with 12 cores and 256 Gb memory. (Our joint inversion code is not parallelized, but we ran 2-4 inversions simultaneously.) We believe that our method is an effective and efficient workaround for 3D joint inverse problems before Monte Care sampling methods can be readily applied to hundreds of thousands of model parameters on PCs.

7 Conclusions

Geology differentiation aims to identify different geological units based on geophysical inverted physical property models. However, analyzing uncertainty of these geophysically derived geological units in 3D has bee not attempted. We have developed an empirical method to construct 3D probabilistic quasi-geology models based on mixed L_p norm joint inversion and prior petrophysical measurements. Our method can be readily applied to many other regions and problems. Our work has broad implications for 3D (probabilistic) geological model building based on multiple geophysical data sets.

8 Acknowledgments and Data Availability Statement

We would like to thank Benjamin Drenth for making drillhole sample measurements available in our research. We acknowledge the SimPEG team for developing the open source package upon which we developed our work. We also thank HPE Data Science Institute at University of Houston for providing the computational resources. The airborne gravity gradient and magnetic data are made publicly available by US Geological Survey and can be accessed via `https://mrdata.usgs.gov/magnetic/show-survey.php?id=IA_10002`.

References

Anderson, J. L. (1983). Proterozoic anorogenic granite plutonism of north america.

Ashwal, L. D. (2010). The temporality of anorthosites. *The Canadian Mineralogist*, *48*(4), 711–728.

Ashwal, L. D. (2013). *Anorthosites* (Vol. 21). Springer Science & Business Media.

Astic, T., Heagy, L. J., & Oldenburg, D. W. (2021). Petrophysically and geologically guided multi-physics inversion using a dynamic gaussian mixture model. *Geophysical Journal International*, *224*(1), 40–68.

Bedrosian, P., Maercklin, N., Weckmann, U., Bartov, Y., Ryberg, T., & Ritter, O. (2007). Lithology-derived structure classification from the joint interpretation of magnetotelluric and seismic models. *Geophysical Journal International*, *170*(2), 737–748.

Cockett, R., Kang, S., Heagy, L. J., Pidlisecky, A., & Oldenburg, D. W. (2015). SimPEG: An open source framework for simulation and gradient based parameter estimation in geophysical applications. *Computers and Geosciences*, *85*, 142–154. Retrieved from `http://dx.doi.org/10.1016/j.cageo.2015.09.015` doi: 10.1016/j.cageo.2015.09.015

Devriese, S. G., Davis, K., & Oldenburg, D. W. (2017). Inversion of airborne geophysics over the do-27/do-18 kimberlites—part 1: Potential fields. *Interpretation*, *5*(3), T299–T311.

Doetsch, J., Linde, N., Coscia, I., Greenhalgh, S. A., & Green, A. G. (2010). Zonation for 3d aquifer characterization based on joint inversions of multimethod crosshole geophysical data. *Geophysics*, *75*(6), G53–G64.

Drenth, B. J., Anderson, R. R., Schulz, K. J., Feinberg, J. M., Chandler, V. W., & Cannon, W. F. (2015). What lies beneath: geophysical mapping of a concealed precambrian intrusive complex along the iowa–minnesota border. *Canadian Journal of Earth Sciences*, *52*(5), 279–293.

Fournier, D., Kang, S., McMillan, M. S., & Oldenburg, D. W. (2017). Inversion of airborne geophysics over the do-27/do-18 kimberlites—part 2: Electromagnetics. *Interpretation*, *5*(3), T313–T325.

Fournier, D., & Oldenburg, D. W. (2019). Inversion using spatially variable mixed Lp norms. *Geophysical Journal International*, *218*(1), 268–282. doi: 10.1093/gji/ggz156

Gallardo, L. A., & Meju, M. A. (2003). Characterization of heterogeneous near-surface materials by joint 2D inversion of dc resistivity and seismic data. *Geophysical Research Letters*, *30*(13), 2–5. doi: 10.1029/2003GL017370

Giraud, J., Lindsay, M., Jessell, M., & Ogarko, V. (2020). Towards plausible lithological classification from geophysical inversion: honouring geological principles in subsurface imaging. *Solid Earth*, *11*(2), 419–436.

Heagy, L. J., Cockett, R., Kang, S., Rosenkjaer, G. K., & Oldenburg, D. W. (2017). A framework for simulation and inversion in electromagnetics. *Computers and Geosciences*, *107*(June), 1–19. Retrieved from `http://dx.doi.org/10.1016/j.cageo.2017.06.018` doi: 10.1016/j.cageo.2017.06.018

Infante, V., Gallardo, L. A., Montalvo-Arrieta, J. C., & de León, I. N. (2010). Litho-

logical classification assisted by the joint inversion of electrical and seismic data at a control site in northeast mexico. *Journal of Applied Geophysics*, *70*(2), 93–102.

Kang, S., Fournier, D., & Oldenburg, D. W. (2017). Inversion of airborne geophysics over the do-27/do-18 kimberlites—part 3: Induced polarization. *Interpretation*, *5*(3), T327–T340.

Kim, D. J., Sun, J., & Melo, A. (2020). Regional scale mineral exploration through joint inversion and geology differentiation based on multi-physics geoscientific data. In *Seg technical program expanded abstracts 2020* (pp. 1379–1383). Society of Exploration Geophysicists.

Li, K., Wei, X., & Sun, J. (2021). Geophysical characterization of a buried niobium and rare earth element deposit using 3d joint inversion and geology differentiation: A case study on the elk creek carbonatite. In *First international meeting for applied geoscience & energy* (pp. 1256–1260).

Li, Y., Melo, A., Martinez, C., & Sun, J. (2019). Geology differentiation: A new frontier in quantitative geophysical interpretation in mineral exploration. *The Leading Edge*, *38*(1), 60–66.

Linde, N., Binley, A., Tryggvason, A., Pedersen, L. B., & Revil, A. (2006). Improved hydrogeophysical characterization using joint inversion of cross-hole electrical resistance and ground-penetrating radar traveltime data. *Water Resources Research*, *42*(12).

Linde, N., Tryggvason, A., Peterson, J. E., & Hubbard, S. S. (2008). Joint inversion of crosshole radar and seismic traveltimes acquired at the south oyster bacterial transport site. *Geophysics*, *73*(4), G29–G37.

Manassero, M. C., Afonso, J. C., Zyserman, F., Zlotnik, S., & Fomin, I. (2020). A reduced order approach for probabilistic inversions of 3-d magnetotelluric data i: general formulation. *Geophysical Journal International*, *223*(3), 1837–1863.

Martinez, C., & Li, Y. (2015). Lithologic characterization using airborne gravity gradient and aeromagnetic data for mineral exploration: A case study in the quadrilátero ferrífero, brazil. *Interpretation*, *3*(2), SL1–SL13.

Melo, A. T., Sun, J., & Li, Y. (2017). Geophysical inversions applied to 3d geology characterization of an iron oxide copper-gold deposit in brazil. *Geophysics*, *82*(5), K1–K13.

Miller, C. A., Christenson, B. W., Byrdina, S., Vandemeulebrouck, J., Brakenrig, T., Britten, K., ... Epstein, G. (2020). Snapshot of a magmatic/hydrothermal system from electrical resistivity tomography and fumarolic composition, whakaari/white island, new zealand. *Journal of Volcanology and Geothermal Research*, *400*, 106909.

Piana Agostinetti, N., & Bodin, T. (2018). Flexible Coupling in Joint Inversions: A Bayesian Structure Decoupling Algorithm. *Journal of Geophysical Research: Solid Earth*, *123*(10), 8798–8826. doi: 10.1029/2018JB016079

Sun, J., Melo, A. T., Kim, J. D., & Wei, X. (2020). Unveiling the 3d undercover structure of a precambrian intrusive complex by integrating airborne magnetic and gravity gradient data into 3d quasi-geology model building. *Interpretation*, *8*(4), SS15–SS29.

Trevino, S. F., Miller, C. A., Tikoff, B., Fournier, D., & Singer, B. S. (2021). Multiple, coeval silicic magma storage domains beneath the laguna del maule volcanic field inferred from gravity investigations. *Journal of Geophysical Research: Solid Earth*, *126*(4), e2020JB020850.

Wei, X., & Sun, J. (2021). Uncertainty analysis of 3d potential-field deterministic inversion using mixed l p norms. *Geophysics*, *86*(6), 1–103.

Zhang, X., Curtis, A., Galetti, E., & De Ridder, S. (2018). 3-d monte carlo surface wave tomography. *Geophysical Journal International*, *215*(3), 1644–1658.